Free Radical Biology and Medicine 65 (2013) 882–894

Contents lists available at ScienceDirect

Free Radical Biology and Medicine

journal homepage: www.elsevier.com/locate/freeradbiomed

Original Contribution

Mitochondria are targets for peroxisome-derived oxidative stress in cultured mammalian cells

Bo Wang [a], Paul P. Van Veldhoven [a], Chantal Brees [a], Noemí Rubio [b], Marcus Nordgren [a], Oksana Apanasets [a], Markus Kunze [c], Myriam Baes [d], Patrizia Agostinis [b], Marc Fransen [a,*]

[a] Laboratory of Lipid Biochemistry and Protein Interactions, Katholieke Universiteit Leuven, 3000 Leuven, Belgium
[b] Laboratory of Cell Death Research and Therapy, Department of Cellular and Molecular Medicine, Katholieke Universiteit Leuven, 3000 Leuven, Belgium
[c] Center for Brain Research, Medical University of Vienna, 1090 Vienna, Austria
[d] Laboratory of Cell Metabolism, Department of Pharmaceutical and Pharmacological Sciences, Katholieke Universiteit Leuven, 3000 Leuven, Belgium

ARTICLE INFO

Article history:
Received 3 June 2013
Received in revised form
13 August 2013
Accepted 19 August 2013
Available online 27 August 2013

Keywords:
Peroxisomes
Mitochondria
Organelle cross-talk
Oxidative stress
Redox signaling
Lipid peroxidation
Cell death
Free radicals

ABSTRACT

Many cellular processes are driven by spatially and temporally regulated redox-dependent signaling events. Although mounting evidence indicates that organelles such as the endoplasmic reticulum and mitochondria can function as signaling platforms for oxidative stress-regulated pathways, little is known about the role of peroxisomes in these processes. In this study, we employ targeted variants of the genetically encoded photosensitizer KillerRed to gain a better insight into the interplay between peroxisomes and cellular oxidative stress. We show that the phototoxic effects of peroxisomal KillerRed induce mitochondria-mediated cell death and that this process can be counteracted by targeted overexpression of a select set of antioxidant enzymes, including peroxisomal glutathione *S*-transferase kappa 1, superoxide dismutase 1, and mitochondrial catalase. We also present evidence that peroxisomal disease cell lines deficient in plasmalogen biosynthesis or peroxisome assembly are more sensitive to KillerRed-induced oxidative stress than control cells. Collectively, these findings confirm and extend previous observations suggesting that disturbances in peroxisomal redox control and metabolism can sensitize cells to oxidative stress. In addition, they lend strong support to the ideas that peroxisomes and mitochondria share a redox-sensitive relationship and that the redox communication between these organelles is not only mediated by diffusion of reactive oxygen species from one compartment to the other. Finally, these findings indicate that mitochondria may act as dynamic receivers, integrators, and transmitters of peroxisome-derived mediators of oxidative stress, and this may have profound implications for our views on cellular aging and age-related diseases.

Introduction

Peroxisomes are highly dynamic cell organelles that play key roles in multiple metabolic pathways [1]. In mammals, these include—among others—the breakdown of various carboxylates via α- and β-oxidation and the biosynthesis of docosahexaenoic acid and ether phospholipids [2,3]. Many of the enzymes involved in these processes produce reactive oxygen species (ROS)[1] as part of their normal catalytic activity [4]. Mammalian peroxisomes also contain various ROS-detoxifying enzymes, including catalase (EC 1.11.1.6, CAT), Cu/Zn-superoxide dismutase 1 (EC 1.15.1.1, SOD1), glutathione *S*-transferase kappa 1 (EC 2.5.1.18, GSTK1), epoxide hydrolase 2 (EC 3.3.2.10), and peroxiredoxin 5 (EC 1.11.1.15) [5]. The importance of peroxisomes for human health and development is best illustrated by the existence of severe inherited metabolic diseases (e.g., Zellweger syndrome and X-linked adrenoleukodystrophy) that are caused by a partial or complete dysfunction of the organelle [6,7]. In addition, there is growing evidence for the involvement of peroxisomes in the etiology and progression of aging and age-related diseases [8]. This may not be so surprising given that changes in peroxisomal metabolism have been suggested to orchestrate developmental decisions (e.g., cell fate) by modulating the cellular composition and concentration of specific lipids and (redox-derived) signaling mediators [9,10]. Unfortunately, little is known about the identity of these signaling pathways and how peroxisomes are integrated into subcellular communication networks [11].

Abbreviations: ALS, amyotrophic lateral sclerosis; c, cytosolic; CAT, catalase; ER, endoplasmic reticulum; GSTK1, glutathione *S*-transferase kappa 1; HuF, human fibroblast; KR, KillerRed; LA, α-lipoic acid; MEF, mouse embryonic fibroblast; mt, mitochondrial; NAC, *N*-acetylcysteine; PARP, poly(ADP-ribose) polymerase; po, peroxisomal; RIPK1, receptor-interacting protein kinase 1; ROS, reactive oxygen species; SOD1, superoxide dismutase 1

* Corresponding author. Fax: +32 16 330642.
E-mail address: marc.fransen@med.kuleuven.be (M. Fransen).

0891-5849/$ - see front matter © 2013 Elsevier Inc. All rights reserved.
http://dx.doi.org/10.1016/j.freeradbiomed.2013.08.173

To fulfill their functions, peroxisomes physically and functionally interact with other cell organelles, including mitochondria, the endoplasmic reticulum (ER), and lipid droplets [1,12]. For example, it is well established that, in mammals, peroxisomes and mitochondria are metabolically linked [13], cooperate in antiviral signaling and defense [14], and share key components of their division machinery [15]. We and others recently found that a disturbance in peroxisomal metabolism triggers signaling/communication events that ultimately result in increased mitochondrial stress [16–18]. In addition, we observed that generating excess ROS inside peroxisomes quickly perturbs the mitochondrial redox balance and leads to excessive mitochondrial fragmentation [16]. The molecular mechanisms underlying these phenomena remain unclear. However, in this context, it is of interest to note that a recent confocal microscopy study has visualized a membrane network, distinct from the ER, which physically connects peroxisomes and mitochondria [19]. These contact sites may facilitate both signaling and the passage of ions and lipids from one compartment to another [20]. On the other hand, it may also be possible that peroxisomal ROS simply diffuse through the peroxisomal membrane via PXMP2, a nonselective pore-forming membrane protein with an upper molecular size limit of 300–600 Da [21]. Finally, it should be mentioned that there is also evidence of a vesicular transport pathway from mitochondria to peroxisomes [22]. However, no data currently exist for such a pathway in the opposite direction.

In this study, we employed a peroxisomal variant of KillerRed (KR), a red fluorescent protein that displays strong phototoxic properties upon green light illumination [23], to gain a better insight into the downstream cellular effects of excess peroxisomal ROS production. In addition, we compared these effects with those of cytosolic and mitochondrial variants of KR. Importantly, previous studies have already shown that targeted variants of KR can be used as powerful tools to study the downstream effects of local ROS production. For example, it has been demonstrated that a membrane-tethered version of this genetically encoded photosensitizer can be used to manipulate the viability and/or function of KR-expressing cells in transgenic zebrafish [24]. Others have shown that mitochondrial KR can be used to robustly initiate parkin-mediated autophagy in a spatially and temporally controlled fashion [25] and to expand our understanding of the role of mitochondrial oxidative stress in cell fate decisions [26,27].

We show here that peroxisomal KR can be used to gain a better insight into factors that may contribute to or influence redox signaling between peroxisomes and mitochondria. Our findings provide strong novel evidence that (i) disturbances in peroxisomal metabolism sensitize cells to KR-induced oxidative stress, (ii) excessive peroxisomal ROS production elicits mitochondria-mediated cell death, and (iii) the redox communication between peroxisomes and mitochondria involves complex signaling pathways. The implications of these findings for how peroxisomes can be integrated into cellular communication networks are discussed.

Materials and methods

DNA manipulations and plasmids

The plasmids encoding nontagged versions of human SOD1 and $SOD1_{G93A}$ were kindly provided by Dr. L. Van Den Bosch (Laboratory for Neurobiology, KU Leuven, Belgium). The plasmid encoding green fluorescent protein (GFP)–Bax was kindly provided by Dr. R. J. Youle (National Institutes of Health, Bethesda, MD, USA). The mammalian expression vectors pEGFP-N1 (Clontech), pKillerRed-dmito (Bio-Connect), and pCR2.1 TOPO (Invitrogen) were commercially obtained. The plasmids encoding CAT, po-KR, mt-KR, c-KR, po-roGFP2, mt-roGFP2, or c-roGFP2 have been described elsewhere [16]. The oligonucleotides used to amplify PCR products are listed in Supplementary Table 1. The plasmid encoding cytochrome *c*–EGFP (pMF1807) was constructed by amplifying the cDNA fragment encoding human cytochrome *c* by PCR (template, human liver cDNA library; primers, HsCytc.fw1 and HsCytc.rv1; nested primers, HsCytc.fwBglII and HsCytc.rvHindIII) and cloning the *Bgl*II/*Hin*dIII-digested PCR product into the *Bgl*II/*Hin*dIII-cut pEGFP-N1 vector. The plasmid encoding nontagged po-CAT (pMF1526), a human catalase variant containing a strong peroxisomal targeting signal, was generated by ligating the PCR-amplified HsCatalase-SKL cDNA fragment (template, pJK18 [28]; primers, HsCatalase.1fwBglII and pBADHisrvNotIPstI; digested with *Bgl*II/*Pst*I) into the *Bgl*II/*Pst*I-cut pEGFP-N1 vector. The construct encoding mt-CAT (pMF1763) was generated by ligating the PCR-amplified HsCatalaseΔKANL cDNA fragment (template, pJK20 [28]; primers, HsCatalase.1fwBglII and pBADHisrevNotIPstI; digested with *Bgl*II/*Not*I) into the *Bgl*II/*Not*I-cut backbone fragment of pKillerRed-dmito. The plasmid encoding mt-SOD1 (pOI19) was created by cloning the PCR-amplified human SOD1 cDNA fragment (template, nontagged HsSOD1 (see above); primers, SOD1fw-BamHI and SOD1revNotI; digested with *Bam*HI/*Not*I) into the *Bam*HI/*Not*I-cut backbone fragment of pKillerRed-dmito. The mammalian expression vector encoding 3xmyc-tagged po-SOD1 (pOI17) was constructed by ligating the PCR-amplified SOD1-SKL cDNA fragment (template, nontagged HsSOD1 (see above); primers, SOD1fwBamHI and SOD1PTS1rvNotI; digested with *Bam*HI/*Not*I) into the *Bam*HI/*Not*I-digested pMP1 plasmid [29]. The plasmid encoding $SOD1_{H46R}$ (pBW2) was constructed by fusion PCR. In a first PCR, two PCR fragments (template, nontagged HsSOD1; primers, SOD1fwBamHI and SOD1H46Rrv (fragment 1) or SOD1H46Rfw and SOD1rvNotIBglII (fragment 2)) were generated. These fragments were fused and used as templates in a second PCR (primers, SOD1fwBamHI and SOD1rvNotIBglII). After digestion with *Bam*HI/*Not*I, the fusion fragment was subcloned into the *Bam*HI/*Not*I-cut backbone fragment of the pEGFP-N1 vector. To generate the plasmid encoding HsGSTK1-roGFP2-PTS1 (pKM1558), the PCR-amplified cDNA fragment encoding HsGSTK1 (template, human cDNA pool; primers, oli_1015 and oli_1828) was subcloned into pCR2.1 via TOPO-TA cloning, and the open reading frame was subsequently excised with *Bgl*II and *Hin*dIII and cloned into the *Bgl*II/*Hin*dIII-cut plasmid encoding peroxisomal roGFP2. The plasmid encoding $HsGSTK1_{S16A}$-roGFP2-PTS1 (pKM1620) was generated by in vitro mutagenesis of plasmid pKM1558 using the Quikchange in vitro mutagenesis kit (Agilent) in combination with the oligonucleotides oli_1872 and oli_1873. The construct encoding mitochondrial HsGSTK1-roGFP2 (pKM1691) was generated via a three-point ligation of the following fragments: (i) the *Nde*I/*Bsr*GI-cut backbone fragment of pEGFP-N1; (ii) the *Nde*I/*Bgl*II-cut fragment of pKM1132, a pEGFP-N1 derivative encoding the 32-amino-acid mitochondrial targeting signal of human ornithine transcarbamoylase; and (iii) the *Bgl*II/*Bsr*GI-cut fragment of pKM1620, which encodes HsGSTK1-roGFP2. All plasmids were verified by DNA sequencing (LGC Genomics).

Antibodies

The mouse monoclonal antibody against β-actin (Sigma), the rabbit polyclonal antibodies against cleaved caspase-3 (Cell Signaling) and poly(ADP-ribose) polymerase (PARP; Cell Signaling), and the goat anti-mouse and anti-rabbit IgGs coupled to alkaline phosphatase (Sigma) were commercially obtained. Note that the anti-PARP antibody recognizes both the full-length protein (~116 kDa) and the large fragment of PARP (~85 kDa) resulting from caspase cleavage.

Cell culture, transfections, and fluorescence microscopy

The immortalized Pex19p-deficient human fibroblasts (HuFs) were kindly provided by Dr. G. Dodt (University of Tübingen, Germany). Control HuFs were obtained from Dr. D. Cassiman (Hepatology, KU Leuven). The *Pex5*$^{+/+}$ and *Pex5*$^{-/-}$ mouse embryonic fibroblasts (MEFs) have been described elsewhere [16,30]. The Bax/Bak control and double-knockout MEFs were kindly provided by Dr. L. Scorrano (Dulbecco-Telethon Institute, Italy) [31]. Glycerone-phosphate *O*-acyltransferase (GNPAT)-deficient MEFs were generated from 14-day-old *Gnpat*$^{-/-}$ embryos [32,33], and the depletion of plasmalogens relative to the phospholipid content in these cells was confirmed by HPLC (*Gnpat*$^{-/-}$ fibroblasts, $\pm$2.2 pmol/nmol; *Gnpat*$^{+/+}$ fibroblasts, $\pm$68 pmol/nmol) [34]. All primary cells were immortalized by introduction of the SV40 large T-antigen upon arrival in the laboratory. Unless specified otherwise, all cells were cultured at 37 °C in a humidified 5% CO_2 incubator in minimum essential medium Eagle α (Bio-Whittaker) supplemented with 10% (v/v) heat-inactivated South American fetal calf serum (Invitrogen), 2 mM Glutamax (Invitrogen), and 0.2% Mycozap (Lonza). The cells were transfected via electroporation as described before [16] and kept in the dark as much as possible. To monitor the transfection efficiencies, a small aliquot of the cells was stained with Hoechst 33342 (5 μg/ml) to visualize all nuclei, and the percentage of cells expressing KR was determined by counting at least 50 randomly selected cells. Cells for live-cell imaging were seeded and imaged in FD-35 FluoroDish cell culture dishes (World Precision Instruments). To distinguish apoptosis from necrosis by fluorescence microscopy, the cells were incubated with Hoechst 33342 (5 μg/ml) and propidium iodide (5 μg/ml) for 30 min at 37 °C, washed 3× with phosphate-buffered saline (PBS), and replenished with regular medium supplemented with 1 μg/ml of each dye. To visualize caspase-3 activity in real time, the cells were incubated with 5 μM NucView 488 (Biotium) for 30 min before illumination with green light. To visualize lipid peroxidation, the cells were incubated for 30 min at 37 °C with 1 μM C11-Bodipy 581/591 (Molecular Probes) in growth medium and washed twice with Dulbecco's PBS before imaging. Fluorescence was evaluated on a motorized inverted IX-81 microscope, controlled by Cell-M software and equipped with a temperature-, humidity-, and CO_2-controlled incubation chamber. The technical specifications of the objectives, excitation and emission filters, and digital camera have been described elsewhere [35]. Changes in the oxidation state of the roGFP2 proteins were determined as described elsewhere [16]. Note that, as the spectral outputs of xenon arc replacement lamps are not identical, the emission ratios of roGFP2 at the 400- and 480-nm excitation wavelengths are different from some of the values reported before [16]. However, as roGFP2 is a ratiometric probe, this does not affect the outcome and conclusions of these studies. The Olympus image analysis and particle detection software was used for quantitative image analysis.

Light irradiation

For the viability, Western blot, and lipid peroxidation assays, the cells were respectively cultivated in 96-well cell culture plates (Greiner Bio-One), 35-mm cell culture dishes (Sarstedt), and FD-35 FluoroDishes (World Precision Instruments) and irradiated with green light (irradiance ~10 mW/cm^2) by using a KL 1500 LCD light source with a green insert filter (Schott). Light flux was measured with an IL1400 radiometer equipped with a SEL033 detector (International Light). The light intensities were corrected for the illuminated area to calculate incident light. To investigate the potential mechanisms of cell death, the cells were incubated in the presence or absence of z-VAD-FMK (20 μM) or necrostatin-1 (30 μM), starting from 1 h before illumination until the cell viability and proliferation assay. To study the effects of pro- and antioxidants on po-KR-induced cell death, the cells were incubated in the presence or absence of L-buthionine-sulfoximine (100 μM), *N*-acetylcysteine (1 mM), α-lipoic acid (0.5 mM), Trolox (2 mM), or L-histidine (5 mM), starting from 24 h before illumination until the cell viability and proliferation assay. To study the effects of KR-mediated ROS production by fluorescence microscopy, the cells were cultivated in FD-35 FluoroDishes and irradiated with green light (100× oil objective, 545–580 nm, irradiance ~10 or ~30 W/cm^2) as specified in each experiment. To calculate the light dose (J/cm^2), the irradiance (W/cm^2) was multiplied by the exposure time (s).

Assessment of cell viability and proliferation

Cell viability was evaluated using the 3-(4,5-dimethylthiazol-2-yl)-2,5-diphenyltetrazolium bromide (MTT) assay. Briefly, 2 or 3 days posttransfection, $\pm 5 \times 10^3$ cells/well were seeded into a 96-well culture plate (8 wells per condition; 200 μl medium per well) and cultivated for 1 day under standard conditions (see above). Next, 4 of the 8 wells were illuminated with green light (see above; the control conditions were wrapped with aluminum foil) for the indicated time periods, and the cells were allowed to grow for an additional 24 h. Then, 20 μl MTT (5 mg/ml in PBS) was added to each well, and the cells were reincubated at 37 °C to allow viable cells to produce formazan. After 4 h, the medium was replaced by 150 μl dimethyl sulfoxide and the cell plate was vibrated for 10 min at room temperature to dissolve the formazan precipitates. The absorbance of the colored solution was measured at 570 nm using a VersaMax microplate reader (Molecular Devices). A reference wavelength of 690 nm was used to correct for any turbidity in the samples. The relative cell viability was expressed as the ratio (%) of the absorbance ($OD_{570\ nm} - OD_{690\ nm}$) in the illuminated wells to that of the corresponding nonilluminated wells. At least two independent experiments were performed for each condition. The transfection efficiencies were determined by fluorescence microscopy (see above).

Statistical analysis

Statistics were performed on the VassarStats statistical computation Web site (http://vassarstats.net/). One-way analysis of variance was used to determine the differences among independent groups of numerical values, and individual differences were further explored with a Student *t* test. Three significance levels were chosen: $p > 0.05$ (no significant difference), $p < 0.05$ (medium significance), and $p < 0.01$ (high significance).

Results

Development and validation of a cell-based assay for studying the effects of KillerRed-induced oxidative stress

Recently, we validated the usefulness of targeted variants of KR to locally increase the redox state in various mammalian cell compartments at the microscopic level [16]. Here we modified and scaled up this microscopy protocol to evaluate the effects of KR-induced oxidative stress at the biochemical level (for more details, see Materials and methods). To validate this new assay, we (i) determined whether peroxisomal, mitochondrial, or cytosolic KR could render its local redox environment more oxidative upon green light illumination and (ii) examined how such treatment affected cell growth and survival. To monitor changes in the subcellular redox state, we employed targeted variants of roGFP2

[16]. This protein is a redox-sensitive variant of the enhanced green fluorescent protein and contains engineered cysteine residues on adjacent surface-exposed strands that form a disulfide bond under oxidizing conditions [36]. As (i) roGFP2 has two fluorescence excitation maxima at ~400 and ~490 nm and (ii) disulfide formation leads to an increase in the excitation peak at ~400 nm at the expense of the ~490 nm peak, the ratio of roGFP2 emissions (at ~510 nm) can provide a nondestructive readout of the redox environment of the fluorophore [36]. The typical distribution patterns of all KR and roGFP2 fusion proteins that are used in this study are shown in Supplementary Fig. S1.

The results of these validation experiments demonstrated that the new experimental setup is suited to generate oxidative stress in specific subcellular compartments (Fig. 1A) and that all KR variants sensitize immortalized mouse embryonic fibroblasts for green-light-induced cell death (Fig. 1B). This phototoxicity was dependent on the subcellular localization of KR (Fig. 1B) and the light dose (Supplementary Fig. S2). As described before [23], c-KR and mt-KR provoked respectively a weak and a strong phototoxic effect. The toxicity of po-KR was comparable to, albeit slightly less severe than, that of mt-KR (Fig. 1B and Supplementary Fig. S2). In this context, it is important to mention that (i) the cellular expression levels of po-KR and mt-KR are comparable, but considerably lower than, that of c-KR (Supplementary Fig. S3) and (ii) essentially similar results were obtained for immortalized human fibroblasts and MIN6 mouse insulinoma cells (data not shown). Note that our finding that po-KR and mt-KR show comparable phototoxicities may be expected from our previous observations that KR-induced ROS production inside peroxisomes quickly disturbs the mitochondrial redox balance and results in excessive mitochondrial fragmentation [16], two indicators of the activation of mitochondrial stress pathways [37].

ROS generated by po-KR induce caspase-dependent and -independent cell death

To gain a better insight into the cell death mechanisms induced by po-KR, we first examined the effects of z-VAD-FMK and necrostatin-1. Z-VAD-FMK is a broad-spectrum inhibitor of caspases, the main executioners of apoptosis [38], and necrostatin-1 is a specific inhibitor of receptor-interacting protein kinase 1 (RIPK1), a kinase whose activity is crucial for necroptosis [39]. These experiments showed that incubating the cells with z-VAD-FMK, starting from 1 h before illumination, significantly—but not completely—abrogated po-KR-induced cell death (Fig. 2A, left). This finding suggests a picture in which po-KR exerts long-term phototoxicity through activation of both caspase-dependent and -independent cell death pathways. Interestingly, treating the cells with necrostatin-1 had no protective effect (Fig. 2A, left), thus suggesting that po-KR-mediated caspase-independent cell death is not caused by a RIPK1-dependent mechanism. For comparison purposes, we also included conditions under which KR was located in the mitochondria or the cytosol. For mt-KR, we obtained results essentially similar to those for po-KR (Fig. 2A, middle). Note that this finding is in line with a recent study showing that z-VAD-FMK can partially protect cells against mt-KR-induced cell death [26]. For c-KR, we did not observe any protective effect of z-VAD-FMK or necrostatin-1 (Fig. 2A, right). However, given the relatively small differences between the values of the illuminated and nonilluminated conditions, this negative result may be due to the small sample size or the slower kinetics of cell death induction (see below).

Next, to strengthen our observation that po-KR can induce apoptosis, we also investigated whether (i) cells lacking both Bax and Bak, two proapoptotic proteins that govern mitochondrial outer membrane permeabilization and subsequent caspase activation [40], are more resistant to po-KR-induced cell death and (ii) po-KR-induced ROS production can result in the cleavage of procaspase-3 and PARP, two markers for apoptosis. The viability

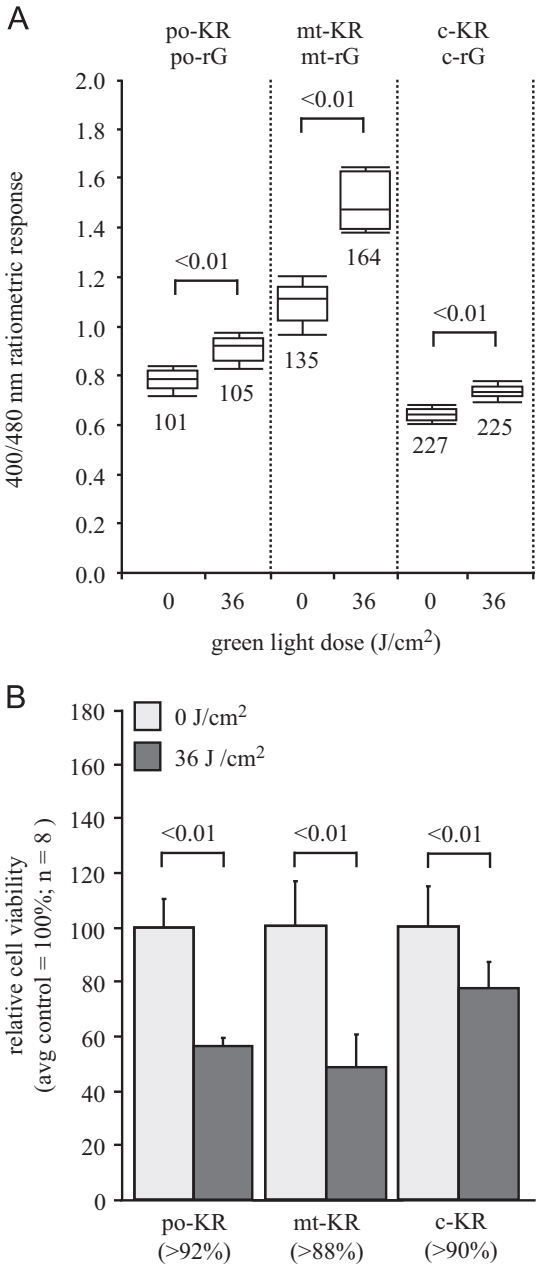

Fig. 1. Validation of a new experimental setup to generate KR-induced oxidative stress inside various subcellular compartments. Immortalized mouse embryonic fibroblasts were transiently cotransfected with plasmids encoding peroxisomal (po-KR), mitochondrial (mt-KR), or cytosolic (c-KR) KillerRed and peroxisomal (po-rG), mitochondrial (mt-rG), or cytosolic (c-rG) roGFP2 and cultured in standard growth medium. After 3 days, the cells were exposed or not to green light (irradiance 10 mW/cm^2) and (A) immediately processed for imaging or (B) 24 h later, subjected to an MTT assay. (A) Box plot representation of the 400/480 nm fluorescence response ratios. The bottom and top of each box represent the 25th and 75th percentile values, respectively; the horizontal line inside each box represents the median; and the horizontal lines below and above each box represent respectively the mean minus and plus 1 standard deviation. The number of measurements is indicated below each box. The values obtained from the illuminated and nonilluminated conditions were evaluated and found to be statistically significant. (B) Effect of the subcellular localization of KR on cell toxicity. The cell viability was expressed as a percentage of the average value of the corresponding nonilluminated condition. The transfection efficiency of each condition is indicated in parentheses. The values obtained from the illuminated and nonilluminated conditions were statistically compared.

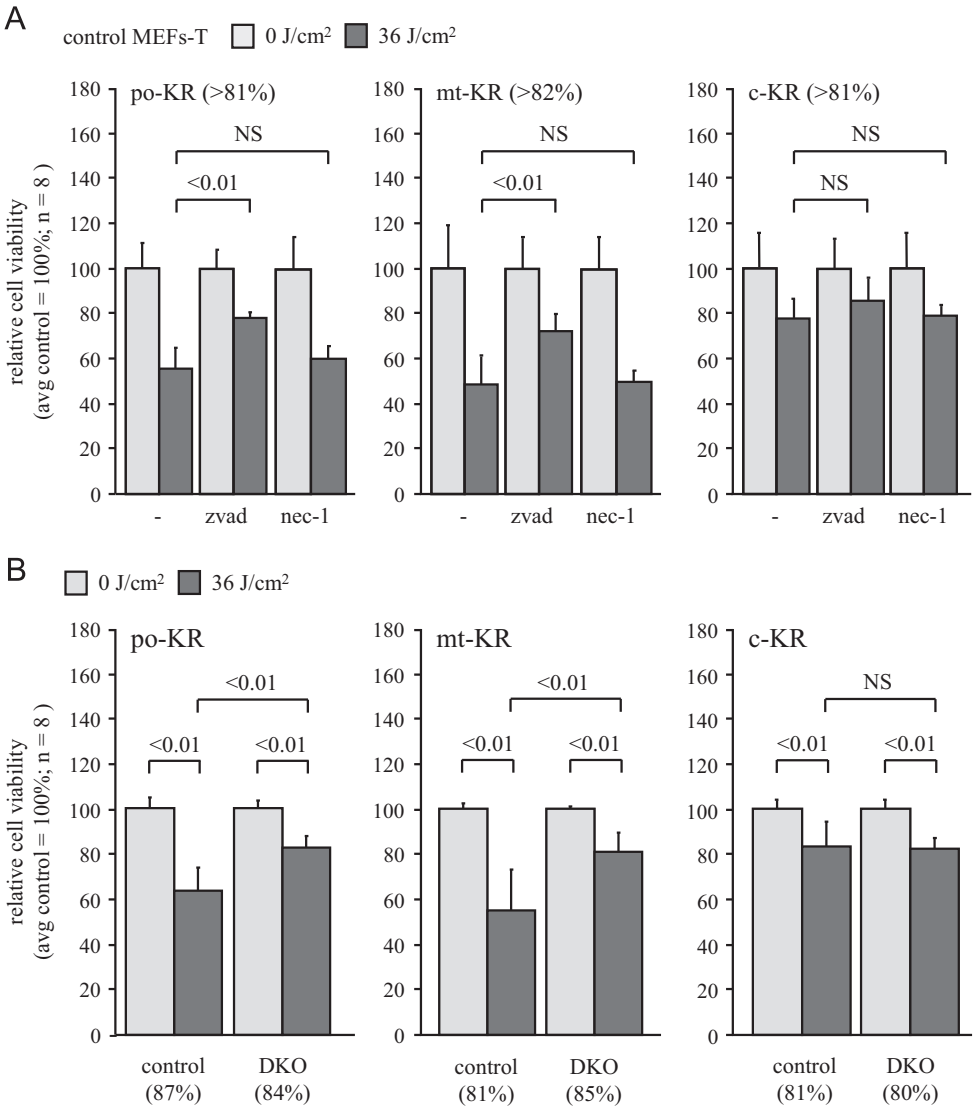

Fig. 2. Cytoprotective effects of cell death inhibitors and Bax/Bak inactivation on KR-induced cell killing. Control and Bax/Bak double-knockout (DKO) immortalized mouse embryonic fibroblasts (MEFs-T) were transiently transfected with a plasmid encoding peroxisomal (po-KR), mitochondrial (mt-KR), or cytosolic (c-KR) KR and cultured in standard growth medium. After 3 days, the cells were exposed or not exposed to green light (irradiance ~10 mW/cm^2). Cell viability was evaluated by MTT assay at 24 h postillumination and expressed as a percentage of the average value of the corresponding nonilluminated condition. The transfection efficiencies are indicated in parentheses. (A) Effects of cell death inhibitors. The cells were incubated in the absence (−) or presence of z-VAD-FMK (zvad; 20 μM) or necrostatin-1 (nec-1; 30 μM), starting from 1 h before illumination until the cell viability assay was carried out. The values obtained from the illuminated inhibitor-treated and illuminated untreated conditions were statistically compared. (B) Bax/Bak-deficient cells were partially protected against KR-induced cell death. The data were statistically compared. NS, nonsignificant.

experiments with the Bax/Bak double-knockout (DKO) cells showed that these cells were partially protected against the phototoxic effects of po-KR and mt-KR (Fig. 2B, left and middle). For c-KR, no significant differences could be observed between the DKO and the control cells (Fig. 2B, right). From our immunoblot data, it is clear that KR-induced oxidative stress results in the cleavage of procaspase-3 into its processed, active form and of its downstream substrate PARP (Fig. 3). Importantly, the kinetics of cleavage are faster for po-KR (~8–16 h postillumination) and mt-KR (~8–16 h postillumination) than for c-KR (~16–24 h postillumination). In sum, these findings along with our z-VAD-FMK studies (compare Figs. 2A and 2B) point to the involvement of a mitochondrial pathway of caspase activation in the mechanism of cell death induced by mt-KR and po-KR.

Finally, as it is well known that cellular responses to light-activated photosensitizers can depend, among other factors, on the total administered dose, the total light exposure dose, the light fluence rate, and the number of pulses [41], we also documented how the cells responded to po-KR-mediated ROS production under our previous microscopic experimental setup [16]. For these experiments, the cells were exposed to a 10-s pulse of green light (irradiance ~30 W/cm^2) once every 30 min. We first studied the morphological changes cells undergo upon expression and photoactivation of po-KR. Therefore, the cells were preincubated with Hoechst 33342, a membrane-permeative nucleic acid stain, and propidium iodide, a membrane-impermeative fluorescent stain that labels only nucleic acids of membrane-compromised cells. These experiments revealed that po-KR-mediated ROS production induced some typical morphological features of apoptosis, including chromatin condensation, plasma membrane blebbing, and the loss of membrane integrity during the late apoptotic stage (Supplementary Fig. S4, left). Note that (i) irradiating the cells with these higher light doses (i.e., microscopic setup) was accompanied by profound KR photobleaching [23] and (ii) the morphological changes induced by po-KR-mediated ROS production could be counteracted by z-VAD-FMK (Supplementary Fig. S4, right).

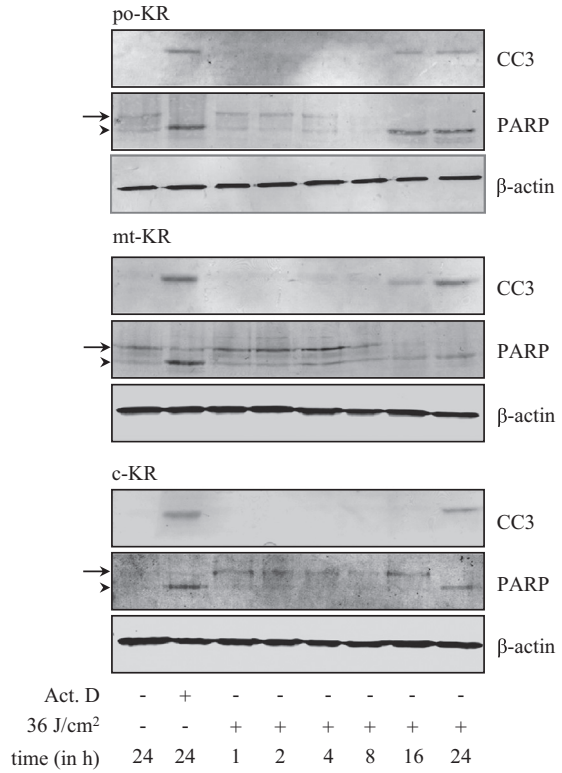

Fig. 3. Effects of KR-induced ROS production on caspase-3 and PARP cleavage. Immortalized mouse embryonic fibroblasts were transiently transfected with a plasmid encoding peroxisomal (po-KR), mitochondrial (mt-KR), or cytosolic (c-KR) KillerRed and cultured in standard growth medium. After 3 days, the cells were incubated with actinomycin D (Act. D; 80 nM; positive control) or exposed (+) or not (−) to green light (irradiance ~10 mW/cm^2). Samples were collected at the indicated time points, total cell extracts were prepared, and equal amounts of the cell extracts were subjected to SDS–PAGE and blotted onto nitrocellulose. The blots were processed for immunostaining with antibodies specific for cleaved caspase-3 (CC3), PARP, and β-actin. The arrows and arrowheads respectively mark full-length and cleaved PARP.

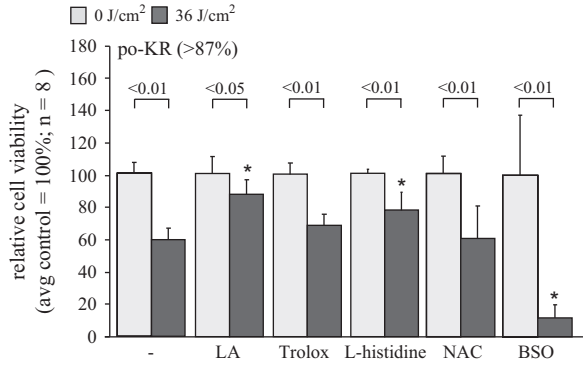

Fig. 4. Effects of pro- and antioxidants on po-KR-induced cell death. Immortalized mouse embryonic fibroblasts were transiently transfected with a plasmid encoding peroxisomal KR (po-KR) and cultured in standard growth medium. After 2 days, the cells were preincubated for 24 h in medium supplemented without (−) or with α-lipoic acid (LA; 0.5 mM), Trolox (2 mM), L-histidine (5 mM), *N*-acetylcysteine (NAC; 1 mM), or L-buthionine-sulfoximine (BSO; 100 μM) and subsequently exposed or not exposed to green light (irradiance ~10 mW/cm^2). Cell viability was evaluated by MTT assay at 24 h postillumination and expressed as the percentage of the average value of the corresponding nonilluminated condition. The values obtained from the illuminated and nonilluminated conditions were evaluated and found to be statistically significant ($p < 0.01$ or $p < 0.05$). The transfection efficiency is indicated in parentheses. The values from the treated illuminated conditions were also statistically compared with the result from the untreated illuminated (control) condition (*$p < 0.01$).

Next, we investigated whether or not po-KR-mediated ROS production could also trigger the movement of Bax from the cytosol to the mitochondria and the subsequent release of cytochrome *c* from the mitochondria into the cytosol, two key events of mitochondrial apoptosis [42]. To this end, we coexpressed po-KR along with GFP–Bax [43] or cytochrome *c*–EGFP [44]. As negative controls, we also included conditions under which GFP–Bax and cytochrome *c*–EGFP were expressed without po-KR. These experiments showed that irradiating the cells with pulses of green light evoked both Bax translocation to (Supplementary Fig. S5) and cytochrome *c* release from mitochondria (Supplementary Fig. S6) in a po-KR-dependent manner. Last, we employed NucView 488, a cell-membrane-permeative fluorogenic caspase-3 substrate [45], to detect KR-induced caspase-3 activity within living cells in real time. Once again, these studies indicate that all KR variants cause caspase-3 activation, with mt-KR inducing the fastest and c-KR the slowest kinetics of caspase-3 activity (Supplementary Fig. S7).

Prevention of po-KR-induced cell death by chemical and enzymatic antioxidants

To further our understanding of how po-KR activation induces mitochondria-mediated cell death, we examined whether this process could be counteracted with chemical antioxidant compounds or by ectopic overexpression of ROS-metabolizing enzymes. In this context, it is important to bear in mind that conflicting data have been reported regarding the types of ROS that are produced by KR: whereas Bulina and co-workers reported that the primary damaging agent generated by KR is singlet oxygen ($^1O_2$) [23], others claim that the cytotoxic effects of this photosensitizer are primarily mediated by other ROS such as superoxide ($O_2^{\bullet -}$) and hydrogen peroxide (H_2O_2) [46,47].

We first included in our assays (i) α-lipoic acid (LA), a naturally occurring compound that scavenges various types of ROS, including $O_2^{\bullet -}$ and $^1O_2$ [48]; (ii) L-histidine, a $^1O_2$ quencher [49]; (iii) Trolox, another $^1O_2$ quencher that can also scavenge peroxyl radicals [50]; and (iv) *N*-acetylcysteine (NAC), a thiol-containing compound that can act as a direct scavenger of $O_2^{\bullet -}$ and H_2O_2 [51]. We found that LA and L-histidine, but not Trolox and NAC, rendered the cells less susceptible to po-KR-induced cell death (Fig. 4). Although these findings clearly demonstrate that chemical antioxidants can interfere with the harmful effects of po-KR-mediated ROS production, they may also be surprising given that LA and NAC are both $O_2^{\bullet -}$ quenchers and that Trolox has been reported to be a better $^1O_2$ scavenger than L-histidine [52]. However, in this context, it should be noted that currently we cannot exclude the possibility that the effective intraperoxisomal concentrations of these antioxidants are different. In addition, as oxidative stress results from complex cascades of radical-generating and radical-scavenging systems, it is important to keep in mind that these antioxidants may provoke cell type- and context-specific responses. Furthermore, these antioxidants may exert their effect by multiple and different mechanisms. For example, whereas NAC can also function as a precursor of reduced glutathione (GSH) [51], LA also acts as an effective redox regenerator of endogenous antioxidants such as vitamin C, vitamin E, and reduced GSH [48]. In this context, it is also relevant to note that a pharmacological depletion of GSH with L-buthionine-(*S,R*)-sulfoximine, a selective inhibitor of glutathione metabolism, sensitized the cells to po-KR-induced cell death (Fig. 4).

Next, we investigated whether po-KR-induced cell death could be counteracted by a select set of antioxidant enzymes. Therefore, we assayed cells overexpressing nontagged human CAT, nontagged human SOD1, or roGFP2-PTS1-tagged human GSTK1: CAT is a predominantly intraperoxisomal enzyme that can degrade H_2O_2 in a catalatic or peroxidatic manner [4], SOD1 is a primarily cytosolic

protein that catalyzes the dismutation of $O_2^{\bullet -}$ to H_2O_2 (this enzyme can also be found in other cellular compartments, including the mitochondrial intermembrane space and the peroxisomal matrix) [4], and (nontagged) GSTK1 is an enzyme that exhibits a bimodal peroxisomal/mitochondrial localization and has GSH-conjugating activity with halogenated aromatics and peroxidase activity toward organic hydroperoxides [53,54]. Importantly, GSTK1-roGFP2-PTS1, the roGFP2-tagged variant of GSTK1 used here, is exclusively targeted to peroxisomes (see below). These experiments showed that overexpression of SOD1 or (po-)GSTK1, but not CAT, provided protection against po-KR-induced cell death (Fig. 5A). This finding suggests that light activation of po-KR gives rise to the local production of $O_2^{\bullet -}$ and lipid peroxides ($LOO^{\bullet}$) as the main toxic ROS.

To further extend and substantiate the interpretation of these observations, we also investigated (i) the effects of overexpression of roGFP2-PTS1-tagged $GSTK1_{S16A}$, a GSTK1 mutant exhibiting 30-fold less activity than the native enzyme [55]; $SOD1_{H46R}$, a mutant of SOD1 lacking superoxide dismutase activity [56]; and $SOD1_{G93A}$, a mutant of SOD1 that has been associated with familial amyotrophic lateral sclerosis (ALS) [57], and (ii) the effectiveness of SOD1, (po-)GSTK1, and CAT at preventing mt-KR- and c-KR-induced cell death. The results of these experiments showed that the S16A substitution in GSTK1-roGFP2-PTS1 and the H46R and G93A substitutions in SOD1 abolished protection against po-KR-induced cell death (Fig. 5A). This outcome was expected for $GSTK1_{S16A}$-roGFP2-PTS1 and $SOD1_{H46R}$. However, for $SOD1_{G93A}$ this observation was rather surprising, given that substitution of glycine to alanine at position 93 has been reported to have little effect on the enzyme's activity [57]. Note that overexpression of (nontagged) $SOD1_{G93A}$ caused mitochondrial fragmentation (Supplementary Fig. S8), an observation already reported by others [58]. Interestingly, only wild-type SOD1 could protect the cells from mt-KR- and c-KR-induced phototoxic cell death (Figs. 5B and 5C). Here, it should be mentioned that, for c-KR, the light dose was increased to 72 J/cm^2 to facilitate the detection of potential differences between the illuminated control and the test conditions.

Finally, to gain a better understanding of how po-KR-mediated ROS production triggers mitochondrial-associated cell death pathways, we also investigated the protective effects of exclusively peroxisome- or mitochondria-matrix-targeted variants of CAT, GSTK1, and SOD1. These experiments yielded two interesting observations: (i) a targeted overexpression of GSTK1 and SOD1, but not CAT, to the KR-containing subcellular compartment rendered the cells less sensitive to green-light-induced cell death (Fig. 6) and (ii) overexpression of mitochondrial, but not peroxisomal, catalase protected the cells against po-KR-mediated ROS production (Fig. 6A). Whereas the first observation confirms the previous finding that H_2O_2 is not the primary ROS released by KR in cellulo [25], the second clearly shows that the type of ROS produced by KR inside peroxisomes differs from the type of ROS that are formed inside mitochondria and cause cell death (Fig. 6A). To unambiguously prove the correctness of our view that po-KR-mediated ROS production results in the generation of H_2O_2 in mitochondria—and not in peroxisomes—we performed additional experiments in which control cells and cells overexpressing mt-CAT were cultivated in the presence of 3-amino-1,2,4-triazole, an inhibitor of catalase activity. These studies clearly showed that inhibition of endogenous (peroxisomal) catalase activity has no effect on cell viability (Fig. 7). From this, we can rule out that the lack of protective benefit of po-CAT overexpression is due to the fact that endogenous catalase, an enzyme known for its remarkably high H_2O_2 turnover number ($\pm 10^6$ molecules/s) [59], is already highly abundant in peroxisomes. In addition, these studies revealed that inhibition of mitochondrial catalase activity resensitizes the cells for po-KR-induced cell death (Fig. 7). From this, we

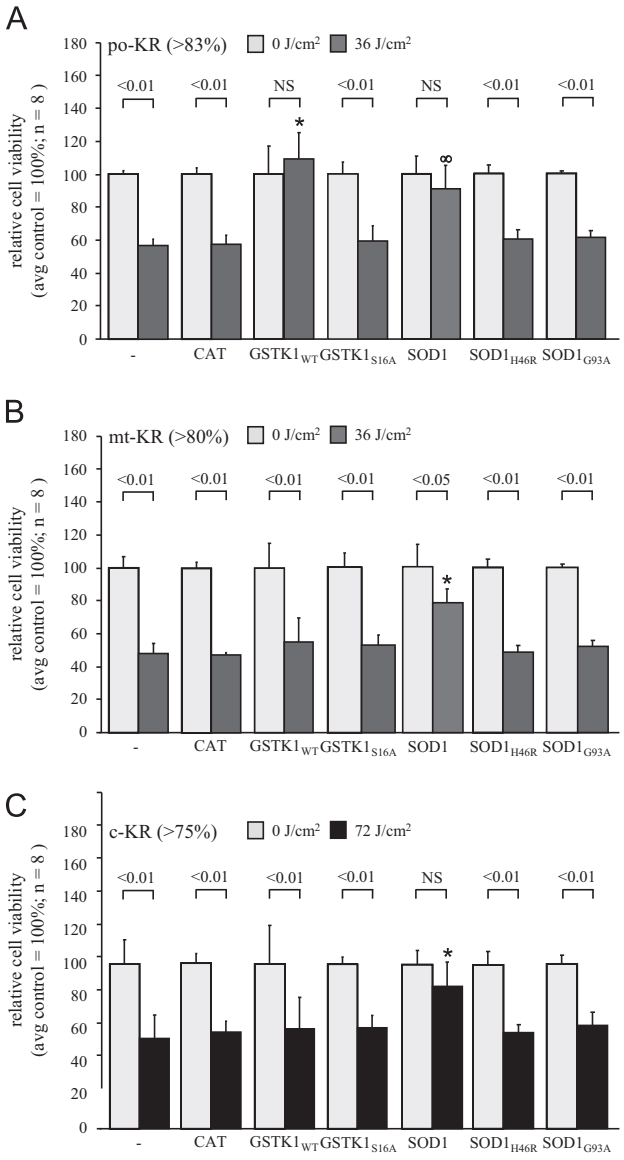

Fig. 5. Effects of overexpression of a select set of antioxidant enzymes on KR-induced cell death. Immortalized mouse embryonic fibroblasts were transiently transfected with a plasmid encoding (A) peroxisomal (po-KR), (B) mitochondrial (mt-KR), or (C) cytosolic (c-KR) KR, in combination or not (−) with a plasmid encoding catalase (CAT), GSTK1-roGFP2-PTS1 ($GSTK1_{WT}$), $GSTK1_{S16A}$-roGFP2-PTS1 ($GSTK1_{S16A}$), superoxide dismutase 1 (SOD1), superoxide dismutase 1_{H46R} ($SOD1_{H46R}$), or superoxide dismutase 1_{G93A} ($SOD1_{G93A}$), and cultured in standard growth medium. After 3 days, the cells were exposed or not exposed to green light (irradiance ~10 mW/cm^2). Cell viability was evaluated by MTT assay at 24 h postillumination and expressed as a percentage of the average value of the corresponding nonilluminated condition. The transfection efficiencies are indicated in parentheses. The values obtained from the illuminated and nonilluminated conditions were evaluated and found to be statistically significant ($p < 0.01$ or $p < 0.05$) or nonsignificant (NS). The values from the illuminated overexpression conditions were also statistically compared with the result from the corresponding illuminated control (−) condition (*$p < 0.01$ or ∞$p < 0.05$).

can conclude with high certainty that po-KR-induced cell death is mediated by mitochondrial-derived H_2O_2.

ROS generated by po-KR promote lipid peroxidation

As (i) there is suggestive evidence that irradiation of KR may cause cell death through excessive lipid oxidation [60,61] and (ii) we obtained indirect evidence that activation of po-KR may give rise to the local production of lipid peroxides (see above), we also

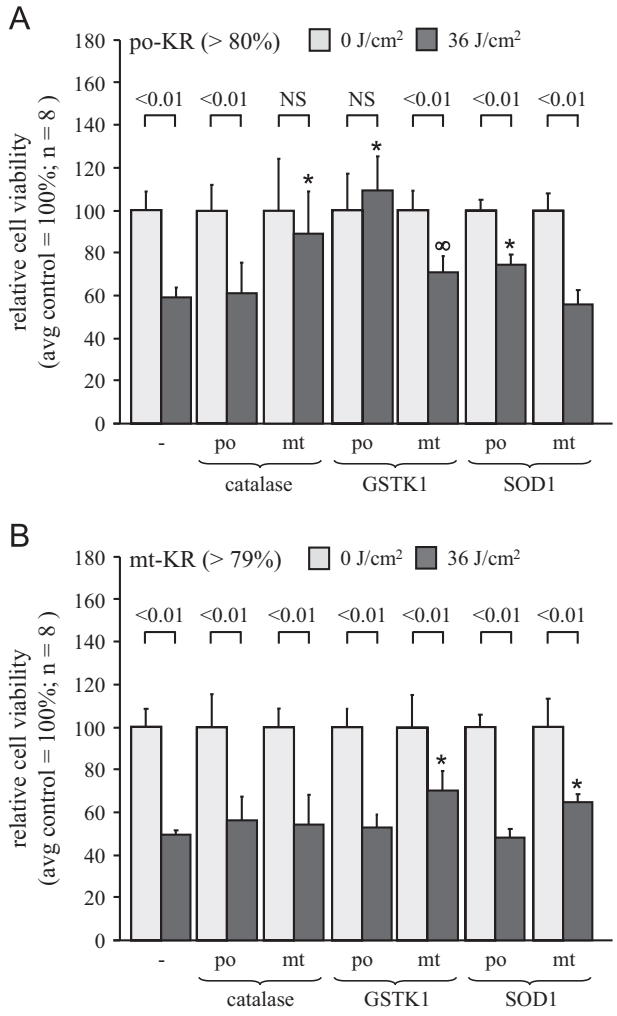

Fig. 6. Effect of the subcellular localization of antioxidant enzymes on KR-induced cell death. Immortalized mouse embryonic fibroblasts were transiently transfected with a plasmid encoding (A) peroxisomal (po-KR) or (B) mitochondrial (mt-KR) KR, in combination or not with a plasmid encoding peroxisomal (po) or mitochondrial (mt) catalase, GSTK1-roGFP2 (GSTK1), or SOD1, and cultured in standard growth medium. After 3 days, the cells were exposed or not exposed to green light (irradiance ~10 mW/cm^2). Cell viability was evaluated by MTT assay at 24 h postillumination and expressed as a percentage of the average value of the corresponding nonilluminated condition. The transfection efficiencies are indicated in parentheses. The values obtained from the illuminated and nonilluminated conditions were evaluated and found to be statistically significant ($p < 0.01$) or nonsignificant (NS). The values from the illuminated overexpression conditions were also statistically compared with results from the corresponding illuminated control (–) condition (*$p < 0.01$ or ∞$p < 0.05$).

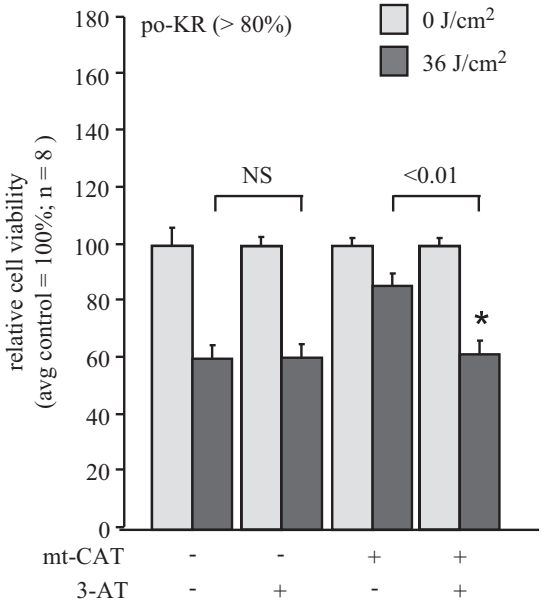

Fig. 7. Effect of pharmacological inhibition of mitochondrial catalase on po-KR-induced cell death. Immortalized mouse embryonic fibroblasts were transiently transfected with a plasmid encoding peroxisomal KR in combination or not with a plasmid encoding mitochondrial catalase and cultured in standard growth medium. After 3 days, the cells were preincubated for 3 h in medium supplemented or not with 3-amino-1,2,4-triazole (3-AT; 10 mM), and subsequently exposed or not exposed to green light (irradiance ~10 mW/cm^2). Cell viability was evaluated by MTT assay at 24 h postillumination and expressed as a percentage of the average value of the corresponding nonilluminated condition. The values obtained from the illuminated treated and untreated conditions were evaluated and found to be statistically significant ($p < 0.01$) or nonsignificant (NS). The transfection efficiency is indicated in parentheses.

tried to find more direct evidence that photoactivation of po-KR does indeed cause cellular lipid peroxidation.

To visualize this process in living cells, we employed C11-Bodipy 581/591, a fluorescent fatty acid analogue in which the Bodipy dye is tethered to a phenol moiety via a diene bond and whose sensitivity to oxidation is comparable to that of endogenous polyunsaturated fatty acyl moieties [62]. C11-Bodipy 581/591 rapidly incorporates into phospholipids of all cellular membranes and—as the red fluorescence (emission peak 595 nm) of the nonoxidized fatty acid analogue shifts to green fluorescence (emission peak 520 nm) upon peroxidation—it can be used as a ratiometric indicator of free radical processes that have the potential to oxidize lipids in membranes [62,63]. However, this probe is not suitable for quantifying lipid peroxidation [63]. Importantly, as (i) C11-Bodipy 581/591 and KR display overlapping red fluorescence emission spectra [23,64] and (ii) peroxidation of C11-Bodipy 581/591 is accompanied by a shift in fluorescence from red to green [62], we monitored lipid peroxidation by processing the cells for live-cell fluorescence imaging in the green channel (Fig. 8). We found that, under standard conditions (and ~30 min after illumination), lipid peroxidation could be consistently detected in approximately 10% of the cells (Fig. 8D). This phenomenon was both KR- and light-dose-dependent (Figs. 8A and C, respectively). For comparison, we also examined the effect of mt-KR and c-KR activation on lipid peroxide formation. For mt-KR, we reliably observed a higher percentage of cells showing a positive (green) staining for oxidized C11-Bodipy 581/591 than for po-KR (Figs. 8E and F). For c-KR, no signs of lipid peroxidation could be detected (Fig. 8H). Note that, as (i) C11-Bodipy 581/591 accumulates in virtually all cellular membranes [64], (ii) this reporter molecule can be the primary target of lipid peroxidation or oxidized by lipid radicals as part of (downstream) propagation reactions [64], and (iii) the activated lipid species may also be exchanged between membranes [65], our experimental setup did not allow us to determine unambiguously in which subcellular compartment the primary lipid radicals are formed and located. However, to gain more insight into this complex issue, we first investigated whether overexpression of GSTK1-roGFP2-PTS1 (po-GSTK1), a green fluorescent protein having the potential to detoxify lipid peroxides [66], could block po-KR- and/or mt-KR-induced lipid peroxidation. From these experiments, it is evident that po-GSTK1 functions only as a lipid peroxidation quencher for po-KR (compare Figs. 8D and 8J with 8F and 8L). Note that, under conditions where po-GSTK1 is expressed, peroxisomes are also visualized in the green channel (Figs. 8I, J, K, and L). However, this peroxisomal staining pattern is clearly different from that observed for the oxidized Bodipy probe (compare Figs. 8D and J).

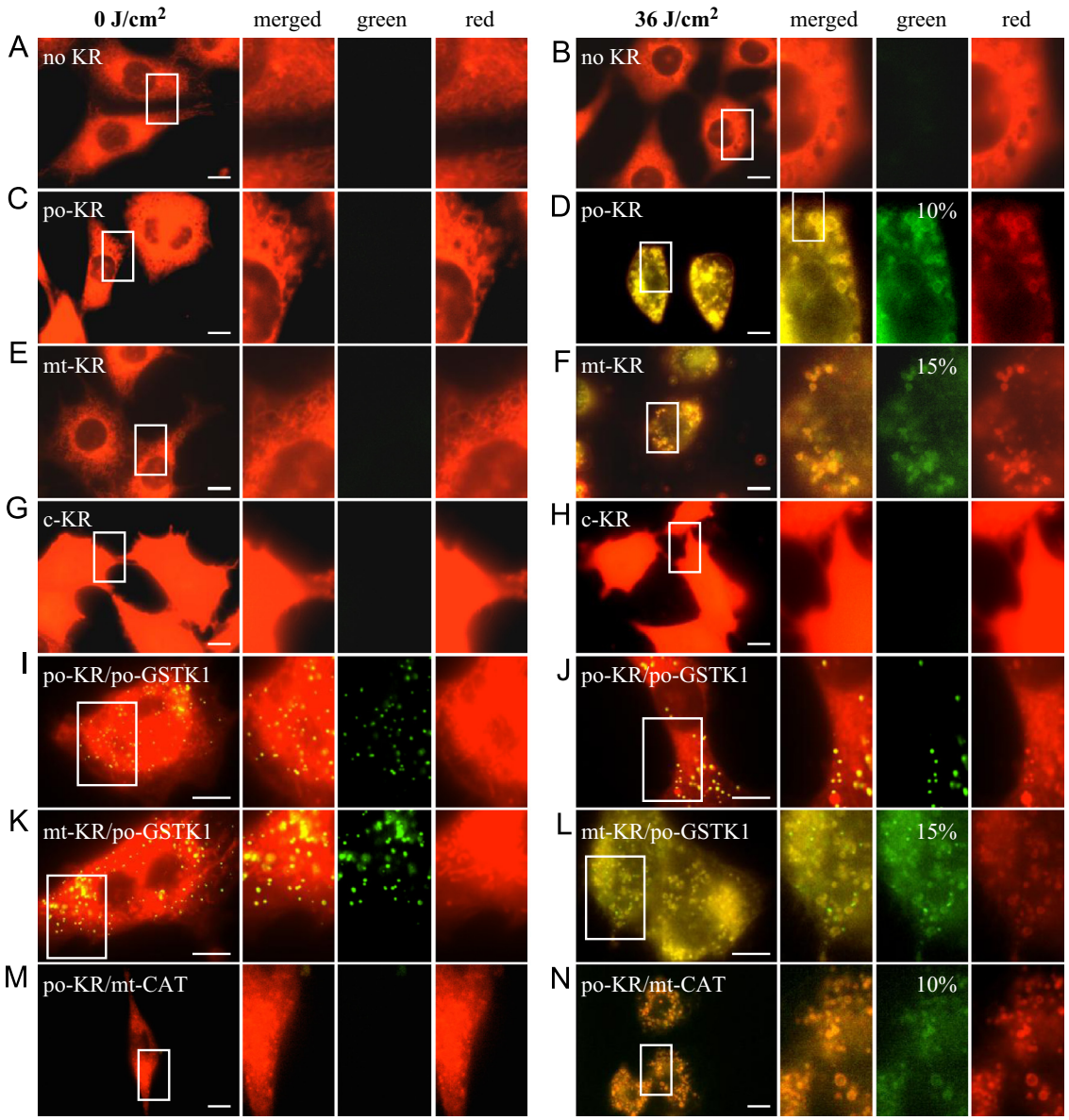

Fig. 8. Detection of KR-induced lipid peroxidation in live cells. Immortalized mouse embryonic fibroblasts were transiently transfected with a plasmid encoding peroxisomal (po-KR), mitochondrial (mt-KR), or cytosolic (c-KR) KR, in combination or not with a plasmid encoding GSTK1-roGFP2-PTS1 (po-GSTK1) or mitochondrial catalase (mt-CAT), and cultured in standard growth medium. After 3 days, the cells were exposed (right) or not exposed (left) to green light (irradiance ~10 mW/cm^2). After illumination, the cells were incubated for 30 min at 37 °C with C11-Bodipy 581/591 (1 μM) in growth medium and processed for fluorescence microscopy (exposure times: red channel, 30 ms; green channel, 200 ms) as described under Materials and methods. Note that (i) C11-Bodipy 581/591 is a lipophilic compound that rapidly incorporates into phospholipids of all cellular membranes; (ii) the emission spectra of the nonoxidized (red) and oxidized (green) forms of C11-Bodipy 581/591 display spectral overlap with KR (red) and (roGFP2-tagged) po-GSTK1 (green), respectively; (iii) the peroxisomal staining pattern of (I, J, K) po-GSTK1 (green) can be easily distinguished from that observed for (D, F, N) the oxidized Bodipy probe (green); and (iv) the green signal in (L) represents a mixture of po-GSTK1 and oxidized C11-Bodipy 581/591.

Next, we also studied the influence of mt-CAT overexpression on po-KR-induced lipid peroxidation. This treatment did not cause any observable changes in lipid peroxidation (compare Figs. 8N and D). As (i) po-GSTK1, but not mt-CAT, can scavenge po-KR-induced lipid peroxidation and (ii) both po-GSTK1 and mt-CAT render cells less susceptible to po-KR-induced cell death (Fig. 6A), these experiments indicate that peroxisome-derived lipid peroxides can activate a cell death pathway in which mitochondria and mitochondrial H_2O_2 production play central roles. This finding is in agreement with our observations that Bax/Bak-deficient cells and z-VAD-FMK, a compound acting downstream of mitochondrial cytochrome *c* release, can (partially) protect cells against po-KR-induced apoptosis (Fig. 2A). Once again, these results point to the idea that the type of oxidative stress generated by po-KR inside peroxisomes differs from the type of oxidative stress that is formed inside mitochondria and causes cell death.

Disturbances in peroxisomal metabolism render the cells more susceptible to KR-induced cell death

In a final series of experiments, we investigated whether a partial or general loss of peroxisome function sensitized the cells to KR-induced cell death. The rationale behind these experiments stems from the observations that (i) Chinese hamster ovary cells deficient in plasmalogen biosynthesis and fibroblasts from patients with peroxisome biogenesis disorders are more sensitive to UV-induced oxidative stress [67,68], (ii) cultured cerebellar neurons from peroxisome-deficient mice display increased oxidative stress

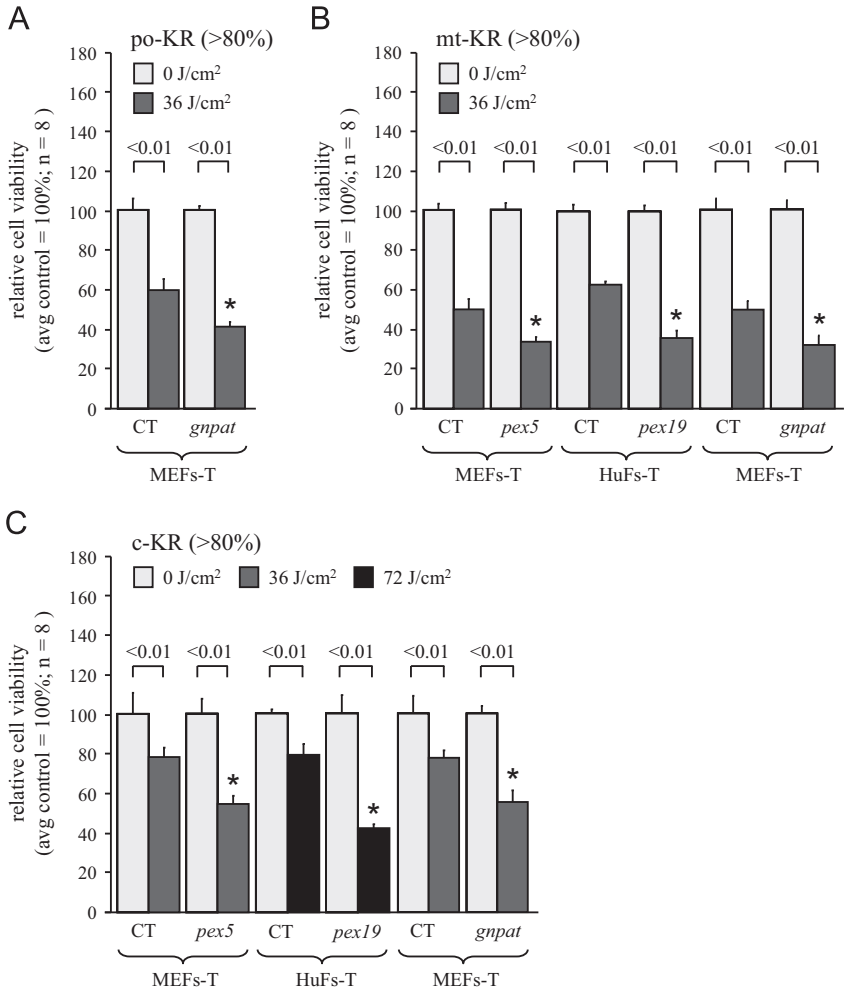

Fig. 9. Disturbances in peroxisomal metabolism sensitize cells to KR-induced cell death. Immortalized mouse embryonic fibroblasts (MEFs-T; CT, control cells; *gnpat*, GNPAT-deficient cells; *pex5*, Pex5p-deficient cells) and human skin fibroblasts (HuFs-T; CT, control cells; *pex19*, Pex19p-deficient cells) were transiently transfected with a plasmid encoding (A) peroxisomal (po-KR), (B) mitochondrial (mt-KR), or (C) cytosolic (c-KR) KR and cultured in standard growth medium. After 3 days, the cells were exposed or not to green light (irradiance ~10 mW/cm^2). Cell viability was evaluated by MTT assay at 24 h postillumination and expressed as a percentage of the average value under the corresponding nonilluminated condition. The transfection efficiencies are indicated in parentheses. The values obtained from the illuminated and nonilluminated conditions were evaluated and found to be statistically significant ($p < 0.01$). The values from the illuminated *pex5*, *pex19*, and *gnpat* cells were also statistically compared with the results from the corresponding illuminated CT cells ($^*p < 0.01$).

and apoptosis [69], and (iii) mouse fibroblasts lacking GNPAT (EC 2.3.1.42), a peroxisomal enzyme catalyzing the first step in ether phospholipid biosynthesis, are more susceptible to 2,2′-azobis(2-methylpropionamidine) dihydrochloride-induced oxidative stress [70]. Note that, as (i) human fibroblasts are less sensitive to KR-induced cell death than mouse fibroblasts (data not shown) and (ii) the phototoxic effects of c-KR are relatively weak (see above), the light dose for the human cells expressing c-KR was increased to 72 J/cm^2 to facilitate the detection of potential differences between the control and the peroxisome-deficient cells.

Our results show that mammalian cells lacking functional peroxisomes or GNPAT activity exhibit an increased sensitivity to KR-induced cell death compared to the corresponding control cells (Fig. 9). To exclude the possibility that the observed differences in cell viability were due to an overall reduction in cellular fitness, we also treated the cells with actinomycin D, a non-ROS-based cytotoxic effector, which can induce cell cycle arrest and apoptosis [71]. Importantly, these experiments did not reveal any difference in the cytotoxicity between control cells and cells lacking functional peroxisomes (Fig. 10). Finally, to gain a better insight into the potential mechanism underlying increased cell mortality, we treated the *Gnpat*$^{-/-}$ cells with z-VAD-FMK or necrostatin-1. These experiments revealed that, also in these cells, (i) the KR fusion proteins exert long-term phototoxicity through activation of both caspase-dependent and -independent cell death pathways and (ii) KR-mediated caspase-independent cell death is not caused by a RIPK1-dependent mechanism (Supplementary Fig. S9). Interestingly, in contrast to the control cells (Fig. 2A), we also found that z-VAD-FMK can partially protect *Gnpat*$^{-/-}$ cells against c-KR-induced cell death (Supplementary Fig. S9). This apparently different behavior can most probably be explained by the fact that *Gnpat*$^{-/-}$ cells are more sensitive to KR-induced oxidative stress (Fig. 9) and that therefore potential differences between the values of the illuminated treated and untreated conditions can be more easily detected. In summary, these findings further establish the peroxisome as an organelle that protects the cell against the adverse effects of ROS from peroxisomal and nonperoxisomal sources.

Discussion

In recent years, strong arguments have been put forward that peroxisomal metabolism and cellular oxidative stress are closely intertwined and that a dysregulation of peroxisome function may

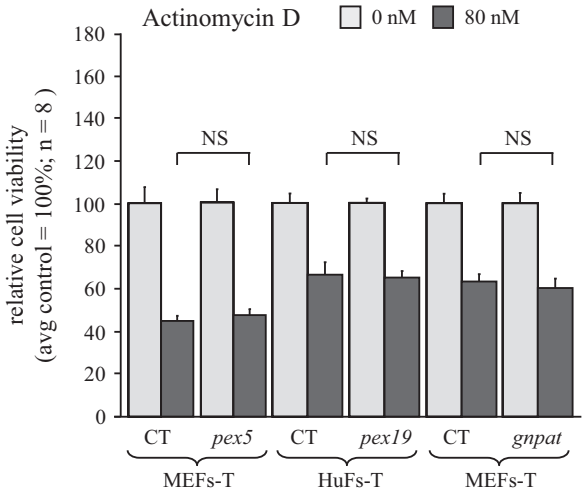

Fig. 10. Disturbances in peroxisomal metabolism do not sensitize cells to actinomycin D-induced cell death. Immortalized mouse embryonic fibroblasts (MEFs-T; CT, control cells; *gnpat,* GNPAT-deficient cells; *pex5,* Pex5p-deficient cells) and human skin fibroblasts (HuFs-T; CT, control cells; *pex19,* Pex19p-deficient cells) were cultured in standard growth medium. After 1 day, the cells were incubated in medium supplemented or not with actinomycin D (80 nM). Cell viability was evaluated by MTT assay at 24 h posttreatment and expressed as a percentage of the average value under the corresponding untreated condition. The values from the treated *pex5, pex19,* and *gnpat* cells were statistically compared with the values from the corresponding treated CT cells. NS, nonsignificant.

contribute to the initiation and progression of human pathologies related to oxidative stress [8,11]. However, the extent to which peroxisomes modulate cytoprotective or cytotoxic responses is not yet clear and has generated much controversy over the years [4]. Here, we employed a peroxisomal variant of KR to investigate how mammalian cells respond to increased ROS production within the peroxisomal matrix.

We found that the production of peroxisomal ROS by the light activation of KR induced cell death in a light dose-dependent manner. This finding extends a previous observation by Elsner et al. [72], who reported that the production of excess H_2O_2 inside peroxisomes can cause β-cell dysfunction and ultimately cell death. By employing various reporter assays, cell lines, and death-preventing agents, we could also show that po-KR-mediated ROS production predominantly activates the caspase-dependent mitochondrial apoptotic pathway. Importantly, as z-VAD-FMK and the absence of both proapoptotic Bax and Bak proteins could not completely counteract the long-term phototoxicity of po-KR, our data also suggest the existence of an alternative, caspase-independent mechanism of cell killing. Interestingly, similar findings were recently reported for mt-KR [26].

Currently, it is generally accepted that both the beneficial and the harmful effects of ROS largely depend on the site, type, and amount of ROS production as well as the activity of the organism's antioxidant defense system [73]. Here, we found that the phototoxic effects of po-KR were more severe than those observed for c-KR, but comparable with those observed for mt-KR. This observation indirectly suggests that the cytotoxic effects of activated po-KR are not simply mediated by the leakage of ROS from peroxisomes into the cytosol. To further analyze the nature and location of po-KR-induced free radical damage, we also conducted a series of experiments in which the cytotoxicity of po-KR and mt-KR was investigated in cells overexpressing a select set of (targeted) antioxidant enzymes. Three important conclusions could be drawn. First, as overexpression of SOD1, but not CAT, (partially) protects the cells from KR-induced phototoxicity when the pro- and antioxidant proteins display similar spatial expression patterns, the main reactive oxygen species involved in the propagation of KR-mediated cell death is most probably $O_2^{\bullet -}$, and not H_2O_2. Second, as GSTK1 shows a protective profile similar to that of SOD1, the $O_2^{\bullet -}$ radicals produced by KR most probably trigger chain reactions in polyunsaturated fatty acids, which lead to membrane lipid peroxidation. Third, as overexpression of mt-CAT —but not po-CAT—can counteract the cytotoxic effects of po-KR, the initial mitochondrial damage resulting from excess peroxisomal ROS is likely to be caused by intramitochondrial H_2O_2. Combined, these results provide a strong foundation for the idea that the redox communication between peroxisomes and mitochondria is part of a complex signaling process and does not simply involve a diffusion of ROS from one compartment to the other. Interestingly, our results also show that the cell-based assay designed here for studying the cytotoxic effects of KR-induced oxidative stress can also be easily adapted to study the in cellulo properties of antioxidant enzymes with ill-defined functions or disease-containing mutations. For example, although human GSTK1, a protein whose expression level has been negatively correlated with obesity [74], has already been shown to exhibit activity toward a number of GST substrates [75], this is—to the best of our knowledge—the first study showing that this enzyme can contribute to lipid peroxide detoxification processes in cellulo. In addition, despite the fact that it has been reported that the ALS-associated mutation G93A in SOD1 has little effect on enzyme activity [57], our data demonstrate that, in contrast to the wild-type protein, $SOD1_{G93A}$ provides no protection to KR-induced oxidative stress. This observation stimulates the need to explore in more depth the mechanisms underlying this and other SOD1 disease-causing mutations.

Over the years, an increasing number of observations have lent support to the concept that a loss of peroxisome function makes cells more vulnerable to oxidative stress [68–70,76]. In this study, we confirm and extend these findings by showing that cells lacking either GNPAT or peroxisomes are more sensitive toward KR-induced oxidative stress than the corresponding control cells. A likely explanation for this difference may be that a partial or complete decrease in peroxisome function will influence the cell's ability to shorten very long chain fatty acids and to synthesize sufficient amounts of plasmalogens [2,3], two processes that are likely to alter membrane composition, structure, fluidity, and function [77,78]. In this context, it is also important to note that plasmalogens are characterized by the presence of a vinyl ether linkage at the *sn*-1 position, and this functionality has been suggested to serve as a sacrificial trap for free radicals [79].

In summary, our observations present strong novel evidence that (i) the presence of functional peroxisomes guards cells against the harmful effects of KR-induced oxidative stress, (ii) excess peroxisomal ROS production elicits mitochondria-mediated cell death, and (iii) the redox communication between peroxisomes and mitochondria involves complex signaling pathways that extend well beyond the simple diffusion of ROS from peroxisomes to mitochondria. As mitochondria represent important metabolic signaling centers that also coordinate various signaling pathways affecting cellular life span [80], these findings have important implications for how we integrate peroxisomes into cellular communication networks during cellular and organismal aging. In this context, it should also be mentioned that (i) a disturbance in the peroxisomal oxidative balance coincides with a depolarization of the mitochondrial inner membrane potential and an increase in mitochondrial ROS production [17] and (ii) dysfunctional peroxisomes impair mitochondrial oxidative phosphorylation and generate mitochondrial ROS in X-linked adrenoleukodystrophy cells [81]. All together, these findings indicate that mitochondria may act as dynamic receivers, integrators, and transmitters of peroxisome-derived oxidative stress. However, many intriguing questions remain. For example, what is the identity of the peroxisomal

oxidative stress messengers, how are these messengers transported from peroxisomes to mitochondria, and how do they trigger mitochondrial ROS production and mitochondrial stress signaling pathways? As, among other examples, there is strong evidence that ER-stress-induced oxidative stress triggers the funneling of Ca^{2+} from the ER to the mitochondria through mitochondria-associated membranes, and this in turn can (i) affect the mitochondrial electron transport chain, (ii) initiate the production of mitochondrial $O_2^{\bullet -}$ and H_2O_2, and (iii) activate mitochondrial-dependent apoptotic pathways [82], fruitful ideas for further work may be gathered from other research disciplines.

Acknowledgments

We thank Dr. W. Just (University of Heidelberg, Germany) for the *Gnpat*$^{+/-}$ mice and Ms. E. De Schryver (LIPIT, KU Leuven, Belgium) for the plasmalogen measurements. This work was supported by grants from the Fonds voor Wetenschappelijk Onderzoek-Vlaanderen (Onderzoeksproject G.0754.09) (to M.F. and P.V.V.) and by KU Leuven Grants OT/09/045 (to M.F. and P.V.V.), DBOF/10/059 (to P.V.V., M.F., and P.A.), and GOA/11/009 (to P.A.). B.W. is supported by a fellowship from the Chinese Research Council.

Appendix A. Supporting information

Supplementary data associated with this article can be found in the online version at http://dx.doi.org/10.1016/j.freeradbiomed.2013.08.173.

References

[1] Fransen, M. Peroxisome dynamics: molecular players, mechanisms, and (dys) functions. *ISRN Cell Biol.* **2012**; 2012. (article ID 714192).
[2] Van Veldhoven, P. P. Biochemistry and genetics of inherited disorders of peroxisomal fatty acid metabolism. *J. Lipid Res.* **51:**2863–2895; 2010.
[3] Braverman, N. E.; Moser, A. B. Functions of plasmalogen lipids in health and disease. *Biochim. Biophys. Acta* **1822:**1442–1452; 2012.
[4] Fransen, M.; Nordgren, M.; Wang, B.; Apanasets, O. Role of peroxisomes in ROS/RNS-metabolism: implications for human disease. *Biochim. Biophys. Acta* **1822:**1363–1373; 2012.
[5] Antonenkov, V. D.; Grunau, S.; Ohlmeier, S.; Hiltunen, J. K. Peroxisomes are oxidative organelles. *Antioxid. Redox Signaling* **13:**525–537; 2010.
[6] Shimozawa, N. Molecular and clinical findings and diagnostic flowchart of peroxisomal diseases. *Brain Dev.* **33:**770–776; 2011.
[7] Waterham, H. R.; Ebberink, M. S. Genetics and molecular basis of human peroxisome biogenesis disorders. *Biochim. Biophys. Acta* **1822:**1430–1441; 2012.
[8] Fransen, M.; Nordgren, M.; Wang, B.; Apanasets, O.; Van Veldhoven, P. P. Aging, age-related diseases and peroxisomes. *Subcell. Biochem.* **69:**45–65; 2013.
[9] Del Río, L. A. Peroxisomes as a cellular source of reactive nitrogen species signal molecules. *Arch. Biochem. Biophys* **506:**1–11; 2011.
[10] Beach, A.; Burstein, M. T.; Richard, V. R.; Leonov, A.; Levy, S.; Titorenko, V. I. Integration of peroxisomes into an endomembrane system that governs cellular aging. *Front. Physiol* **3:**283; 2012.
[11] Titorenko, V. I.; Terlecky, S. R. Peroxisome metabolism and cellular aging. *Traffic* **12:**252–259; 2011.
[12] Kohlwein, S. D.; Veenhuis, M.; van der Klei, I. J. Lipid droplets and peroxisomes: key players in cellular lipid homeostasis or a matter of fat—store 'em up or burn 'em down. *Genetics* **193:**1–50; 2013.
[13] Wanders, R. J. Peroxisomes lipid metabolism, and peroxisomal disorders. *Mol. Genet. Metab.* **83:**16–27; 2004.
[14] Dixit, E.; Boulant, S.; Zhang, Y.; Lee, A. S.; Odendall, C.; Shum, B.; Hacohen, N.; Chen, Z. J.; Whelan, S. P.; Fransen, M.; Nibert, M. L.; Superti-Furga, G.; Kagan, J. C. Peroxisomes are signaling platforms for antiviral innate immunity. *Cell* **141:**668–681; 2010.
[15] Islinger, M.; Grille, S.; Fahimi, H. D.; Schrader, M. The peroxisome: an update on mysteries. *Histochem. Cell Biol* **137:**547–574; 2012.
[16] Ivashchenko, O.; Van Veldhoven, P. P.; Brees, C.; Ho, Y. S.; Terlecky, S. R.; Fransen, M. Intraperoxisomal redox balance in mammalian cells: oxidative stress and interorganellar cross-talk. *Mol. Biol. Cell* **22:**1440–1451; 2011.
[17] Walton, P. A.; Pizzitelli, M. Effects of peroxisomal catalase inhibition on mitochondrial function. *Front. Physiol* **3:**108; 2012.
[18] López-Erauskin, J.; Galino, J.; Bianchi, P.; Fourcade, S.; Andreu, A. L.; Ferrer, I.; Muñoz-Pinedo, C.; Pujol, A. Oxidative stress modulates mitochondrial failure and cyclophilin D function in X-linked adrenoleukodystrophy. *Brain* **135:**3584–3598; 2012.
[19] Horner, S. M.; Liu, H. M.; Park, H. S.; Briley, J.; Gale Jr. M. Mitochondrial-associated endoplasmic reticulum membranes (MAM) form innate immune synapses and are targeted by hepatitis C virus. *Proc. Natl. Acad. Sci. USA* **108:**14590–14595; 2011.
[20] Rosenberger, S.; Connerth, M.; Zellnig, G.; Daum, G. Phosphatidylethanolamine synthesized by three different pathways is supplied to peroxisomes of the yeast *Saccharomyces cerevisiae*. *Biochim. Biophys. Acta* **1791:**379–387; 2009.
[21] Antonenkov, V. D.; Hiltunen, J. K. Transfer of metabolites across the peroxisomal membrane. *Biochim. Biophys. Acta* **1822:**1374–1386; 2012.
[22] Neuspiel, M.; Schauss, A. C.; Braschi, E.; Zunino, R.; Rippstein, P.; Rachubinski, R. A.; Andrade-Navarro, M. A.; McBride, H. M. Cargo-selected transport from the mitochondria to peroxisomes is mediated by vesicular carriers. *Curr. Biol.* **18:**102–108; 2008.
[23] Bulina, M. E.; Chudakov, D. M.; Britanova, O. V.; Yanushevich, Y. G.; Staroverov, D. B.; Chepurnykh, T. V.; Merzlyak, E. M.; Shkrob, M. A.; Lukyanov, S.; Lukyanov, K. A. A genetically encoded photosensitizer. *Nat. Biotechnol.* **24:**95–99; 2006.
[24] Teh, C.; Chudakov, D. M.; Poon, K. L.; Mamedov, I. Z.; Sek, J. Y.; Shidlovsky, K.; Lukyanov, S.; Korzh, V. Optogenetic *in vivo* cell manipulation in KillerRed-expressing zebrafish transgenics. *BMC Dev. Biol.* **10:**110; 2010.
[25] Wang, Y.; Nartiss, Y.; Steipe, B.; McQuibban, G. A.; Kim, P. K. ROS-induced mitochondrial depolarization initiates PARK2/PARKIN-dependent mitochondrial degradation by autophagy. *Autophagy* **8:**1462–1476; 2012.
[26] Shibuya, T.; Tsujimoto, Y. Deleterious effects of mitochondrial ROS generated by KillerRed photodynamic action in human cell lines and *C. elegans*. *J. Photochem. Photobiol. B* **117:**1–12; 2012.
[27] Shirmanova, M. V.; Serebrovskaya, E. O.; Lukyanov, K. A.; Snopova, L. B.; Sirotkina, M. A.; Prodanetz, N. N.; Bugrova, M. L.; Minakova, E. A.; Turchin, I. V.; Kamensky, V. A.; Lukyanov, S. A.; Zagaynova, E. V. Phototoxic effects of fluorescent protein KillerRed on tumor cells in mice. *J. Biophotonics* **6:**283–290; 2013.
[28] Legakis, J. E.; Koepke, J. I.; Jedeszko, C.; Barlaskar, F.; Terlecky, L. J.; Edwards, H. J.; Walton, P. A.; Terlecky, S. R. Peroxisome senescence in human fibroblasts. *Mol. Biol. Cell* **13:**4243–4255; 2002.
[29] Pinto, M. P.; Grou, C. P.; Alencastre, I. S.; Oliveira, M. E.; Sá-Miranda, C.; Fransen, M.; Azevedo, J. E. The import competence of a peroxisomal membrane protein is determined by Pex19p before the docking step. *J. Biol. Chem.* **281:**34492–34502; 2006.
[30] Baes, M.; Gressens, P.; Baumgart, E.; Carmeliet, P.; Casteels, M.; Fransen, M.; Evrard, P.; Fahimi, D.; Declercq, P. E.; Collen, D.; van Veldhoven, P. P.; Mannaerts, G. P. A mouse model for Zellweger syndrome. *Nat. Genet.* **17:**49–57; 1997.
[31] Scorrano, L.; Oakes, S. A.; Opferman, J. T.; Cheng, E. H.; Sorcinelli, M. D.; Pozzan, T.; Korsmeyer, S. J.; BAX, BAK regulation of endoplasmic reticulum Ca^{2+}: a control point for apoptosis. *Science* **300:**135–139; 2003.
[32] Rodemer, C.; Thai, T. P.; Brugger, B.; Kaercher, T.; Werner, H.; Nave, K. A.; Wieland., F.; Gorgas, K.; Just, W. W. Inactivation of ether lipid biosynthesis causes male infertility, defects in eye development and optic nerve hypoplasia in mice. *Hum. Mol. Genet* **12:**1881–1895; 2003.
[33] Krysko, O.; Bottelbergs, A.; Van Veldhoven, P.; Baes, M. Combined deficiency of peroxisomal beta-oxidation and ether lipid synthesis in mice causes only minor cortical neuronal migration defects but severe hypotonia. *Mol. Genet. Metab* **100:**71–76; 2010.
[34] Hulshagen, L.; Krysko, O.; Bottelbergs, A.; Huyghe, S.; Klein, R.; Van Veldhoven, P. P.; De Deyn, P. P.; D'Hooge, R.; Hartmann, D.; Baes, M. Absence of functional peroxisomes from mouse CNS causes dysmyelination and axon degeneration. *J. Neurosci.* **28:**4015–4027; 2008.
[35] Nordgren, M.; Wang, B.; Apanasets, O.; Brees, C.; Veldhoven, P. P.; Fransen, M. Potential limitations in the use of KillerRed for fluorescence microscopy. *J. Microsc.* **245:**229–235; 2012.
[36] Hanson, G. T.; Aggeler, R.; Oglesbee, D.; Cannon, M.; Capaldi, R. A.; Tsien, R. Y.; Remington, S. J. Investigating mitochondrial redox potential with redox-sensitive green fluorescent protein indicators. *J. Biol. Chem.* **279:**13044–13053; 2004.
[37] Seo, A. Y.; Joseph, A. M.; Dutta, D.; Hwang, J. C.; Aris, J. P.; Leeuwenburgh, C. New insights into the role of mitochondria in aging: mitochondrial dynamics and more. *J. Cell Sci.* **123:**2533–2542; 2010.
[38] Vandenabeele, P.; Vanden Berghe, T.; Festjens, N. Caspase inhibitors promote alternative cell death pathways. *Sci. STKE* **2006(358):**pe44; 2006.
[39] Christofferson, D. E.; Yuan, J. Necroptosis as an alternative form of programmed cell death. *Curr. Opin. Cell Biol.* **22:**263–268; 2010.
[40] Buytaert, E.; Callewaert, G.; Vandenheede, J. R.; Agostinis, P. Deficiency in apoptotic effectors Bax and Bak reveals an autophagic cell death pathway initiated by photodamage to the endoplasmic reticulum. *Autophagy* **2:**238–240; 2006.
[41] Buytaert, E.; Dewaele, M.; Agostinis, P. Molecular effectors of multiple cell death pathways initiated by photodynamic therapy. *Biochim. Biophys. Acta* **1776:**86–107; 2007.
[42] Martinou, J. C.; Youle, R. J. Mitochondria in apoptosis: Bcl-2 family members and mitochondrial dynamics. *Dev. Cell* **21:**92–101; 2011.

[43] Wolter, K. G.; Hsu, Y. T.; Smith, C. L.; Nechushtan, A.; Xi, X. G.; Youle, R. J. Movement of Bax from the cytosol to mitochondria during apoptosis. *J. Cell Biol.* **139:**1281–1292; 1997.
[44] Goldstein, J. C.; Waterhouse, N. J.; Juin, P.; Evan, G. I.; Green, D. R. The coordinate release of cytochrome c during apoptosis is rapid, complete and kinetically invariant. *Nat. Cell Biol.* **2:**156–162; 2000.
[45] Cen, H.; Mao, F.; Aronchik, I.; Fuentes, R. J.; Firestone, G. L. DEVD-NucView488: a novel class of enzyme substrates for real-time detection of caspase-3 activity in live cells. *FASEB J* **22:**2243–2252; 2008.
[46] Serebrovskaya, E. O.; Edelweiss, E. F.; Stremovskiy, O. A.; Lukyanov, K. A.; Chudakov, D. M.; Deyev, S. M. Targeting cancer cells by using an antireceptor antibody-photosensitizer fusion protein. *Proc. Natl. Acad. Sci. USA* **106:** 9221–9225; 2009.
[47] Vegh, R. B.; Solntsev, K. M.; Kuimova, M. K.; Cho, S.; Liang, Y.; Loo, B. L.; Tolbert, L. M.; Bommarius, A. S. Reactive oxygen species in photochemistry of the red fluorescent protein Killer Red. *Chem. Commun.* **47:**4887–4889; 2011.
[48] Packer, L.; Witt, E. H.; Tritschler, H. J. Alpha-lipoic acid as a biological antioxidant. *Free Radic. Biol. Med.* **19:**227–250; 1995.
[49] Wade, A. M.; Tucker, H. N. Anti-oxidant characteristics of L-histidine. *J. Nutr. Biochem.* **9:**308–315; 1998.
[50] Bisby, R. H.; Morgan, C. G.; Hamblett, I.; Gormahn, A. A. Quenching of singlet oxygen by trolox C, ascorbate and amino acids: effects of pH and temperature. *J. Chem. Phys. A* **103:**7454–7459; 1999.
[51] Benrahmoune, M.; Thérond, P.; Abedinzadeh, Z. The reaction of superoxide radical with *N*-acetylcysteine. *Free Radic. Biol. Med.* **29:**775–782; 2000.
[52] Arellano, J. B.; Li, H.; González-Pérez, S.; Gutiérrez, J.; Melø, T. B.; Vacha, F.; Naqvi, K. R. Trolox, a water-soluble analogue of α-tocopherol, photoprotects the surface-exposed regions of the photosystem II reaction center *in vitro:* is this physiologically relevant? *Biochemistry* **50:**8291–8301; 2011.
[53] Morel, F.; Rauch, C.; Petit, E.; Piton, A.; Theret, N.; Coles, B.; Guillouzo, A. Gene and protein characterization of the human glutathione S-transferase kappa and evidence for a peroxisomal localization. *J. Biol. Chem.* **279:**16246–16253; 2004.
[54] Robinson, A.; Huttley, G. A.; Booth, H. S.; Board, P. G. Modelling and bioinformatics studies of the human Kappa-class glutathione transferase predict a novel third glutathione transferase family with similarity to prokaryotic 2-hydroxychromene-2-carboxylate isomerases. *Biochem. J* **379:**541–552; 2004.
[55] Ladner, J. E.; Parsons, J. F.; Rife, C. L.; Gilliland, G. L.; Armstrong, R. N. Parallel evolutionary pathways for glutathione transferases: structure and mechanism of the mitochondrial class kappa enzyme rGSTK1-1. *Biochemistry* **43:**352–361; 2004.
[56] Ratovitski, T.; Corson, L. B.; Strain, J.; Wong, P.; Cleveland, D. W.; Culotta, V. C.; Borchelt, D. R. Variation in the biochemical/biophysical properties of mutant superoxide dismutase 1 enzymes and the rate of disease progression in familial amyotrophic lateral sclerosis kindreds. *Hum. Mol. Genet* **8:**1451–1460; 1999.
[57] Gurney, M. E.; Pu, H.; Chiu, A. Y.; Dal Canto, M. C.; Polchow, C. Y.; Alexander, D. D.; Caliendo, J.; Hentati, A.; Kwon, Y. W.; Deng, H. X.; Chen, W. J.; Zhai, P.; Sufit, R. L.; Siddique, T. Motor neuron degeneration in mice that express a human Cu,Zn superoxide dismutase mutation. *Science* **264:**1772–1775; 1994.
[58] Raimondi, A.; Mangolini, A.; Rizzardini, M.; Tartari, S.; Massari, S.; Bendotti, C.; Francolini, M.; Borgese, N.; Cantoni, L.; Pietrini, G. Cell culture models to investigate the selective vulnerability of motoneuronal mitochondria to familial ALS-linked G93A SOD1. *Eur. J. Neurosci.* **24:**387–399; 2006.
[59] Nicholls, P.; Fita, I.; Loewen, P. C. Enzymology and structure of catalases. *Adv. Inorg. Chem.* **51:**51–106; 2000.
[60] Bulina, M. E.; Lukyanov, K. A.; Britanova, O. V.; Onichtchouk, D.; Lukyanov, S.; Chudakov, D. M. Chromophore-assisted light inactivation (CALI) using the phototoxic fluorescent protein KillerRed. *Nat. Protoc.* **1:**947–953; 2006.
[61] Lee, A.; Mathuru, A. S.; Teh, C.; Kibat, C.; Korzh, V.; Penney, T. B.; Jesuthasan, S. The habenula prevents helpless behavior in larval zebrafish. *Curr. Biol.* **20:**2211–2216; 2010.
[62] Drummen, G. P.; van Liebergen, L. C.; Op den Kamp, J. A.; Post, J. A. C11-BODIPY (581/591), an oxidation-sensitive fluorescent lipid peroxidation probe: (micro)spectroscopic characterization and validation of methodology. *Free Radic. Biol. Med.* **33:**473–490; 2002.
[63] MacDonald, M. L.; Murray, I. V.; Axelsen, P. H. Mass spectrometric analysis demonstrates that BODIPY 581/591 C11 overestimates and inhibits oxidative lipid damage. *Free Radic. Biol. Med.* **42:**1392–1397; 2007.
[64] Drummen, G. P.; Gadella, B. M.; Post, J. A.; Brouwers, J. F. Mass spectrometric characterization of the oxidation of the fluorescent lipid peroxidation reporter molecule C11-BODIPY(581/591). *Free Radic. Biol. Med.* **36:**1635–1644; 2004.
[65] Prinz, W. A. Lipid trafficking sans vesicles: where, why, how? *Cell* **143:** 870–874; 2010.
[66] Petit, E.; Michelet, X.; Rauch, C.; Bertrand-Michel, J.; Tercé, F.; Legouis, R.; Morel, F. Glutathione transferases kappa 1 and kappa 2 localize in peroxisomes and mitochondria, respectively, and are involved in lipid metabolism and respiration in *Caenorhabditis elegans*. *FEBS J.* **276:**5030–5040; 2009.
[67] Zoeller, R. A.; Morand, O. H.; Raetz, C. R. A possible role for plasmalogens in protecting animal cells against photosensitized killing. *J. Biol. Chem.* **263:**11590–11596; 1988.
[68] Hoefler, G.; Paschke, E.; Hoefler, S.; Moser, A. B.; Moser, H. W. Photosensitized killing of cultured fibroblasts from patients with peroxisomal disorders due to pyrene fatty acid-mediated ultraviolet damage. *J. Clin. Invest.* **88:**1873–1879; 1991.
[69] Müller, C. C.; Nguyen, T. H.; Ahlemeyer, B.; Meshram, M.; Santrampurwala, N.; Cao, S.; Sharp, P.; Fietz, P. B.; Baumgart-Vogt, E.; Crane, D. I. PEX13 deficiency in mouse brain as a model of Zellweger syndrome: abnormal cerebellum formation, reactive gliosis and oxidative stress. *Dis. Model. Mech* **4:**104–119; 2011.
[70] Brodde, A.; Teigler, A.; Brugger, B.; Lehmann, W. D.; Wieland, F.; Berger, J.; Just, W. W. Impaired neurotransmission in ether lipid-deficient nerve terminals. *Hum. Mol. Genet* **21:**2713–2724; 2012.
[71] Kleeff, J.; Kornmann, M.; Sawhney, H.; Korc, M. Actinomycin D induces apoptosis and inhibits growth of pancreatic cancer cells. *Int. J. Cancer* **86:**399–407; 2000.
[72] Elsner, M.; Gehrmann, W.; Lenzen, S. Peroxisome-generated hydrogen peroxide as important mediator of lipotoxicity in insulin-producing cells. *Diabetes* **60:**200–208; 2011.
[73] Circu, M. L.; Aw, T. Y. Reactive oxygen species, cellular redox systems, and apoptosis. *Free Radic. Biol. Med.* **48:**749–762; 2010.
[74] Liu, M.; Zhou, L.; Xu, A.; Lam, K. S.; Wetzel, M. D.; Xiang, R.; Zhang, J.; Xin, X.; Dong, L. Q.; Liu, F. A disulfide-bond A oxidoreductase-like protein (DsbA-L) regulates adiponectin multimerization. *Proc. Natl. Acad. Sci. USA* **105:** 18302–18307; 2008.
[75] Morel, F.; Aninat, C. The glutathione transferase kappa family. *Drug Metab. Rev.* **43:**281–291; 2011.
[76] Li, X.; Baumgart, E.; Morrell, J. C.; Jimenez-Sanchez, G.; Valle, D.; Gould, S. J. PEX11 beta deficiency is lethal and impairs neuronal migration but does not abrogate peroxisome function. *Mol. Cell. Biol.* **22:**4358–4365; 2002.
[77] Périchon, R.; Bourre, J. M.; Kelly, J. F.; Roth, G. S. The role of peroxisomes in aging. *Cell. Mol. Life Sci.* **54:**641–652; 1998.
[78] Nagura, M.; Saito, M.; Iwamori, M.; Sakakihara, Y.; Igarashi, T. Alterations of fatty acid metabolism and membrane fluidity in peroxisome-defective mutant ZP102 cells. *Lipids* **39:**43–50; 2004.
[79] Wallner, S.; Schmitz, G. Plasmalogens: the neglected regulatory and scavenging lipid species. *Chem. Phys. Lipids* **164:**573–589; 2011.
[80] Schmidt, M.; Kennedy, B. K. Aging: one thing leads to another. *Curr. Biol.* **22:** R1048–R1051; 2012.
[81] Lopez-Erauskin, J.; Galino, J.; Ruiz, M.; Cuezva, J. M.; Fabregat, I.; Cacabelos, D.; Boada, J.; Martinez, J.; Ferrer, I. Pamplona, R.; Villarroya, F.; Portero-Otin, M.; Fourcade, S.; Pujol, A. Impaired mitochondrial oxidative phosphorylation in the peroxisomal disease X-linked adrenoleukodystrophy. *Hum. Mol. Genet* **22:**3296–3305; 2013.
[82] Appenzeller-Herzog, C. Glutathione- and non-glutathione-based oxidant control in the endoplasmic reticulum. *J. Cell Sci* **124:**847–855; 2011.